Batteries & Supercaps

Research Article
doi.org/10.1002/batt.202300398

Chemistry Europe
European Chemical Societies Publishing

www.batteries-supercaps.org

Surface Engineering of Binder-free Anodes of Bi and Cu Compounds with Se and Carbon Nanotubes to Improve Lithium-ion Batteries

Yelyzaveta Rublova,*[a] Xiangze Kong,[b] Vitalijs Lazarenko,[a] Jana Andzane,[a] Raimonds Meija,[a] Arturs Viksna,[c] Tanja Kallio,[b] and Donats Erts[a, c]

This study focuses on the surface engineering of binder-free anodes composed of Bi, Se, Cu, and carbon nanotubes to enhance lithium-ion batteries. The anodes synthesized in this study showed promising electrochemical properties. However, issues with cycle stability, operational speed, and solid electrolyte interface (SEI) formation affected their overall performance. To address these challenges, the study applied different conductive polymers, namely PEO, CMC, and PEGDA-co-VC, to form artificial SEI layers. The application of these polymers altered the stability and efficiency of the electrodes, with the PEGDA-co-VC-coated electrodes demonstrating significant stability and consistent capacity over numerous cycles.

Introduction

With the advent of lithium-ion batteries, materials science received a significant impetus for development.[1–3] Researchers around the world are actively exploring new materials and their processing methods to create more efficient and reliable batteries.[4–8] Particular attention is being paid to anodes, the key elements of a battery, that affect its capacity and stability.[7,9–11] In this context, nanomaterials are emerging as a pivotal tool in the development of advanced energy systems.[12] Nanomaterials can provide a shorter path for ion diffusion, increase the number of ion storage sites, and limit volume change, thereby contributing to enhanced battery performance.[13] Moreover, nanomaterials offer more opportunities for electrode fabrication and device design.[14] Some materials that were once thought to be electrochemically inactive in bulk can demonstrate improved electrochemical performance at the nanoscale.[12] Transition metal chalcogenides, such as selenides, are considered extremely promising for use in lithium-ion batteries anodes due to their unique physical and chemical properties.[15,16] Bismuth selenide (Bi_2Se_3) has attracted considerable attention due to its unique layered structure, high electrical conductivity, and excellent lithium-ion diffusion kinetics.[17–19] However, like other chalcogenide materials, bismuth selenide faces the challenge of volume expansion during lithium-ion intercalation/deintercalation, which can lead to structural degradation and capacity loss during cycling.[20] The low-cost and environmentally friendly copper selenide (Cu_2Se) is another interesting metal chalcogenide that has recently gained interest for applications in lithium-ion batteries.[16,21–23] Due to its excellent electronic conductivity and multiple lithium-ion storage sites, copper selenide exhibits a high theoretical capacitance.[23] More detailed studies are needed on the use of copper selenide as an anode for lithium-ion batteries. A progressive step towards enhancing the performance of chalcogenide anodes and increasing their electrochemical properties involves the use of bimetallic metal selenides, which can exhibit a synergistic effect.[24–27] For instance, Zhu and co-authors[27] demonstrated that compared to the simple Cu_2Se and CoSe electrodes, the Cu_2Se/CoSe composite electrode shows improved capacitive properties with a high specific capacity (108.6 $mAh\,g^{-1}$ at 1 $A\,g^{-1}$). Typically, in creating battery electrodes, the materials are mixed with carbon black and polymer binders and then pressed onto metal substrates.[28,29] However, it is possible to use conductive matrices such as carbon nanotubes (CNT) instead of binders.[30] The absence of a binder allows for maximizing the active material in the anode structure, leading to an increased battery capacity.[28,29,31] Despite the promising properties, several problems remain with such approaches for metal chalcogenide anodes. These include issues with cycle stability, operational speed, and solid electrolyte interface (SEI) formation, which can affect overall battery performance and safety.[32] In response to these challenges, one promising approach for enhancing the performance of metal chalcogenide anodes involves the formation of an artificial SEI layer. Conductive polymers can form a protective layer over the anode, acting as a stable physical barrier that prevents harmful side reactions between the anode material and electrolyte.[33] Besides preventing direct contact between the electrolyte and the electrode, the conductive polymers also allow for efficient

[a] Dr. Y. Rublova, V. Lazarenko, Dr. J. Andzane, Dr. R. Meija, Prof. Dr. D. Erts
Institute of Chemical Physics
University of Latvia
Raina Boulevard 19, LV-1586 Riga (Latvia)
E-mail: yelyzaveta.rublova@lu.lv

[b] Dr. X. Kong, Prof. Dr. T. Kallio
Aalto University
School of Chemical Engineering
Kemistintie 1, 02150, Espoo (Finland)

[c] Prof. Dr. A. Viksna, Prof. Dr. D. Erts
Faculty of Chemistry
University of Latvia
Raina Boulevard 19, LV-1586 Riga (Latvia)

Research Article
doi.org/10.1002/batt.202300398
Chemistry Europe
European Chemical Societies Publishing

lithium-ion transport.[34] This is due to their unique structures, which possess ion channels that facilitate lithium-ion migration.[35] To the best of knowledge, there are no reports on application of conductive polymers for hybrid metal selenides – CNT network-like anodes for the formation of an artificial SEI. The structure of this scientific paper will be organized as follows: initially, there will be an exploration of the application of binder-free Cu_2Se and Bi_2Se_3@SWCNT, as well as bimetallic Cu–Bi selenide@SWCNT anode. Subsequently, advanced techniques of surface engineering of these anodes will be discussed. Surface engineering could potentially enhance the anodes' stability, performance, and compatibility with electrolytes by modifying their surface properties with different conductive polymers. Consideration will be given to polymers that have been previously reported to possess a high capability to uptake Li^+-ions during the first charging cycle: Polyethylene oxide (PEO), Carboxymethyl Cellulose (CMC) and co-polymer of poly(ethylene glycol) diacrylate-co-vinylene carbonate (PEGDA-co-VC).

Results and Discussion

Structure and electrochemical characteristics of electrode materials

The Cu_2Se anode synthesized directly on copper substrate is composed of cubic-shaped crystals ranging in size from 6–10 μm crystals (Figure 1a), which represent monoclinic copper selenide (Figure 1b). This type of copper selenide is characterized by high brittleness and a tendency to peel off from the substrate.

The heterostructure Bi_2Se_3@SWCNT comprises nanoplates of Bi_2Se_3 that are randomly oriented and penetrate the SWCNT network (Figure 1c). Analysis of the diffraction pattern (Figure 1d) confirmed the rhombohedral structure of Bi_2Se_3. with lattice parameters $a = 4.1355$ Å; $c = 28.6150$ Å. The presence of CNT was further indicated by the diffraction peak at 26.15°, confirming the presence of carbon in the product.

The surface of bimetallic Cu–Bi selenide@SWCNT electrode is covered with crystals less than 1 μm in size (Figure 1e). The obtained diffraction peaks corresponded to $Cu_{1.9}Se$ with lattice parameters: $a = 5.7960$ Å (JCPDS 04-019-7889) (Figure 1f).

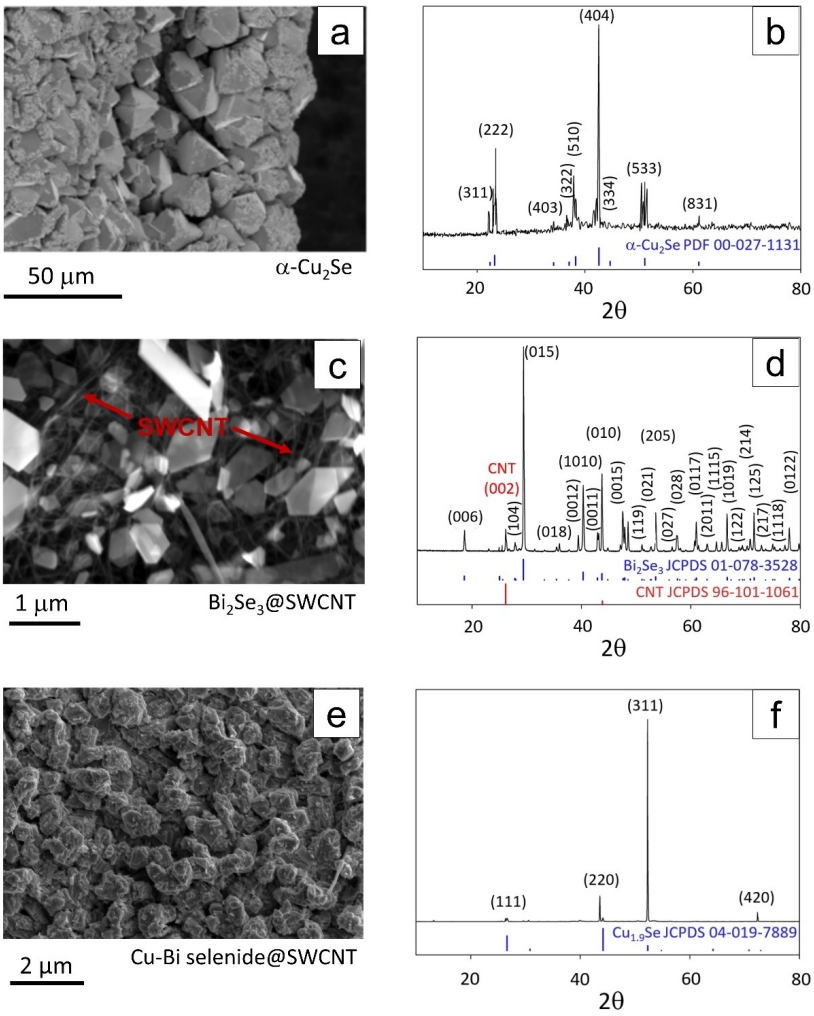

Figure 1. a, c, e) SEM images and b, d, f) XRD patterns for a, b) Cu_2Se, c, d) Bi_2Se_3@SWCNT, and e, f) bimetallic Cu–Bi selenide@SWCNT electrodes.

Research Article
doi.org/10.1002/batt.202300398
Chemistry Europe
European Chemical Societies Publishing

Potentially a smaller crystal size can enhance the electrochemical activity of the material, as it increases the total surface area available for reaction. This can contribute to an increase in the charge/discharge capacity.

The Cu_2Se electrode at 0.1 A g^{-1} has an initial charging capacity of 478 mAh g^{-1} and a discharge capacity of 527 mAh g^{-1} (Figure 2a). After the first three cycles, the discharge and charging capacities become approximately equal, indicating the stabilization of the electrode structure and the formation of optimal paths for electron transfer. However, the capacity significantly decreases more than 25 times during the first 7 cycles, reaching only 18 mAh g^{-1} with a Coulombic efficiency of 92.5%. After 50 cycles the capacity of Cu_2Se electrode slowly decreasing. A strong decrease in capacity may be due to mechanical wear of the brittle electrode and the activation of certain irreversible processes, such as the formation of decomposition products, which degrade conductivity and overall system efficiency.

The electrode, composed of Bi_2Se_3@SWCNT heterostructures, with a Bi_2Se_3 : SWCNT mass ratio of 2:1, demonstrated a higher initial capacity than Cu_2Se. The charge capacity at 0.1 A g^{-1} was measured at 853 mAh g^{-1}, while the initial discharge capacity reached 616 mAh g^{-1}. Over the first 15 cycles, the capacity decreased but then stabilized at 120 mAh g^{-1}, maintaining this level over 500 cycles (Figure 2b). The Coulombic efficiency of the Bi_2Se_3@SWCNT electrode increased from 72% to 100% after 13 cycles. The 100% value was maintained for 500 cycles, indicating stable electrode performance. It should also be noted that by changing the mass ratio of SWCNTs, the electrode capacity can be increased, and at an optimal concentration of Bi_2Se_3:SWCNT (1:1) the discharge capacity reaches 523 mAh g^{-1} after 100 cycles.[36]

The investigation of the electrode composed of bimetallic Cu–Bi selenide@SWCNT (with relative content of SWCNT is 35% by mass) revealed that its initial charge and discharge capacities are 520 mAh g^{-1} (Figure 2c). These values are close to the analogous values for Cu_2Se, although slightly lower. Over the first five cycles, the specific capacity of the electrode decreased approximately threefold (Figure 2c). However, a linear increase in capacity was then observed: the charge capacity increased from 182 mAh g^{-1} in the 5th cycle to 566 mAh g^{-1} after 100 cycles, and the discharge capacity increased from 166 to 373 mAh g^{-1}. The decrease and subsequent increase in the electrode's capacity are associated with forming a protective solid electrolyte interface (SEI) and its initial instability.[37,38] The increase in capacity may be related to the activation of previously inactive electrode materials, especially SWCNT.[39–42] In addition, Se–C bonds can form between the SWCNTs and the unbound selenium. The formed Se–C bonds not only holds the selenium in the electrode but also may provide additional electron paths.[43] The synergy between SWCNT and Se ensures a more efficient electron flow within the electrode, which can lead to the capacitive contribution and overall battery performance. During the first 25 cycles, Coulombic efficiency decreased from 100% to 77%, indicating a more noticeable decline in the early stages of the process. However, after 25 cycles, it continues to decrease, reaching a value of 68% by the 100th cycle. This demonstrates that over time, there is a sustained decrease in Coulombic

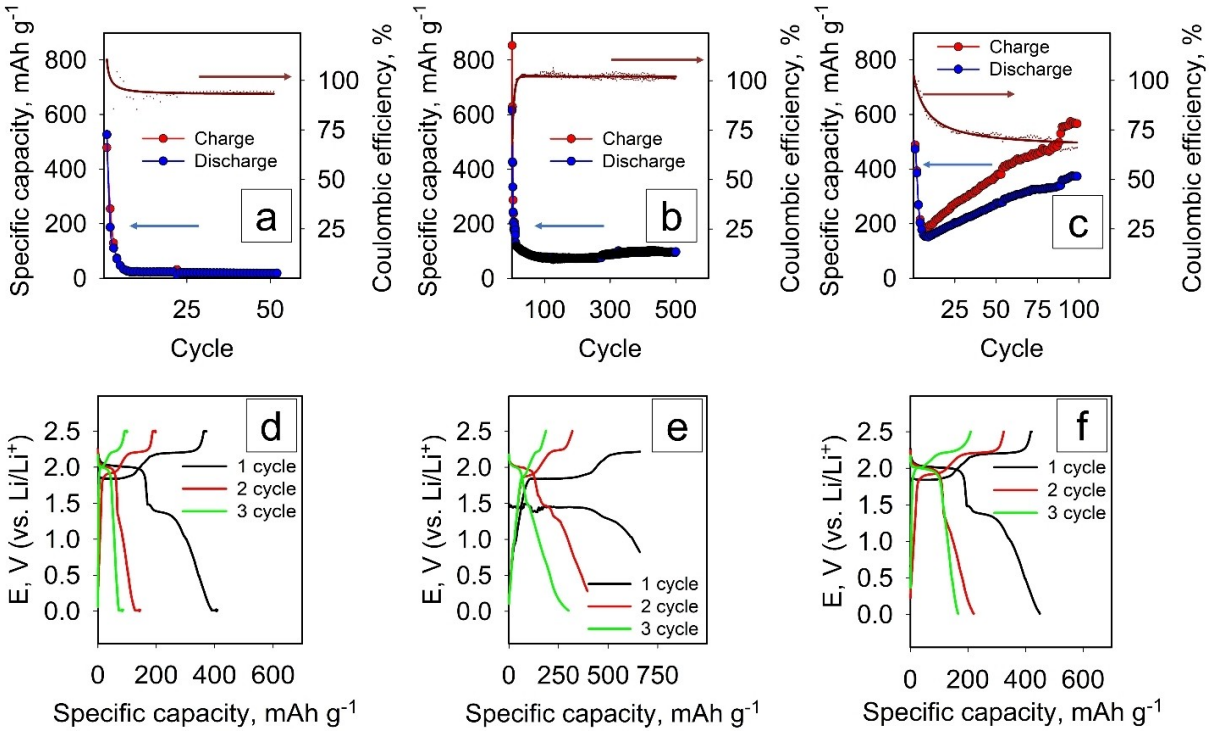

Figure 2. a–c) Cycling performance and d–f) charge-discharge profiles of first 3 cycles for a, d) Cu_2Se, c, d) Bi_2Se_3@SWCNT, and e, f) bimetallic Cu–Bi selenide@SWCNT electrodes electrode at 0.1 A g^{-1}.

efficiency, and it may be necessary to take additional measures to improve it.

For a deeper study of the processes occurring inside the materials, we will consider the charge-discharge profiles in the first three cycles for each of the electrodes. For the Cu_2Se anode, during the first three cycles, two pronounced plateaus are observed at a negative current (Figure 2d). The first plateau, corresponding to a potential of 2.02 V, is associated with the intercalation of Li-ions into the copper selenide structure with the formation of Li_xCuSe.[41] The second plateau, appearing at a potential of 1.4 V, corresponds to the conversion of Cu_2Se to Cu and Li_2Se.[43] By the third cycle, the plateau at 2.02 V disappears, but the plateau at 1.38 V remains, albeit diminished. This could indicate a potential limitation of lithium-ion access to the active anode material. When a positive current is applied, we also observe two plateaus. The first plateau, corresponding to a potential of 1.86 V, is associated with the first stage of the reverse transformation of copper and Li_2Se into Cu_2Se, and the second, wider plateau, corresponding to a potential of 2.24 V, indicates the second stage of this process.[43,44] During the first three cycles, both plateaus are maintained, but their area decreases. This indicates a reduction in the reversibility of the processes that occur during charging, possibly due to degradation of the active material or the formation of non-conductive decomposition products.

For Bi_2Se_3@SWCNT during the first charging cycle at a positive current, plateaus on charge-discharge profiles were observed at 1.82 V and 2.20 V (Figure 2e). These plateaus were associated with the conversion of metallic bismuth into Bi_2Se_3 and lithium deintercalation processes. In subsequent cycles, these plateaus persisted, although their area reduced. When a negative current was applied during the first cycle, the capacity was determined by the process occurring at 1.48 V. This plateau on the charge-discharge profile corresponded to the chemical replacement of bismuth by lithium ($Bi_2Se_3 + xLi^+ + xe \rightarrow Li_xSe_3 + 2Bi$).[18] In subsequent cycles, another plateau appeared at 2.0 V, indicative of lithium intercalation into the van der Waals space of bismuth selenide.[45]

The charge-discharge profiles of the bimetallic Cu–Bi selenide@SWCNT (Figure 2f) were found to be analogous to the charge-discharge profiles of Cu_2Se (Figure 2d). This suggests that the main contribution to capacity accumulation is due to the copper selenide present in the electrode composition.

The study of three electrode materials, Cu_2Se, Bi_2Se_3@SWCNT and bimetallic Cu–Bi selenide@SWCNT, revealed interesting aspects of their electrochemical performance and potential for lithium-ion battery applications (Table 1).

Cu_2Se has a good initial discharge capacity of 527 mAh g^{-1}, but in the first 7 cycles, it decreases to 18 mAh g^{-1}. This result make Cu_2Se electrode less attractive for further research and application in Li-ion batteries.

Bi_2Se_3@SWCNT exhibits outstanding initial capacity (616 mAh g^{-1}) and stability. After coulombic efficiency reaches 100%, indicating reliable performance over 500 cycles. This electrode is a promising candidate as an anode for lithium-ion batteries.

Bimetallic Cu–Bi selenide@SWCNT has an initial capacity close to Cu_2Se (520 mAh g^{-1}), but its capacity increases after an initial decrease, reaching 373 mAh g^{-1} after 100 cycles. The decline in coulombic efficiency suggests a need to improve performance over time, possibly through the creation of an artificial solid electrolyte interface (SEI). The creation of SEI can be a key aspect to further increase capacity and prevent significant capacity loss in the initial cycles for all of these materials

Conductive polymers as artificial SEI layer

Three different types of electrode coating were studied: PEO, CMC, and PEGDA-co-VC. Even though these polymers possess different properties, they all exhibited similar interactions with the crystal structures in our target systems: Bi_2Se_3@SWCNT and Cu–Bi selenide@SWCNT. This finding underlines the universality of these interactions. As an illustration of this phenomenon, we chose the data obtained using the CMC coating (Figure 3). In the Bi_2Se_3@SWCNT system, the polymer forms a shell around the crystals, creating a protective layer. As a demonstration of this phenomenon, we refer to the data obtained using CMC coating, presented in Figure 3. In the Bi_2Se_3@SWCNT system, where randomly oriented Bi_2Se_3 nanoplates penetrate and coat the SWCNT network (Figure 1c), the polymer forms a shell around the crystal clusters, creating a protective layer (Figure 3a). This layer may influence the electrochemical properties of the Bi_2Se_3@SWCNT system, particularly affecting the transport of ions and electrons. Contrastingly, in the Cu–Bi selenide@SWCNT system, the crystals exhibit a cubic structure indicative of copper selenide. Here, the polymer tends to coat individual particles rather than forming a shell around the entire cluster (Figure 3b). This differentiated coating approach might influence surface reactions during charging and dis-

Table 1. Comparison of binder-free Cu_2Se, Bi_2Se_3@SWCNT and bimetallic Cu–Bi selenide@SWCNT electrodes for Li-ion Batteries.

Parameter		Cu_2Se	Bi_2Se_3@SWCNT	Bimetallic Cu–Bi selenide@SWCNT
Discharge capacity, mAh g^{-1}	Initial	527	616	520
	After 50 cycles	18	120	274 (373 after 100th cycle)
Coulombic Efficiency	After 50 cycles	92.5	100.0	73.0
Key Features		Sharp decrease in capacity	Capacity stability over 500 cycles	Increase in capacity during cycling

Research Article
doi.org/10.1002/batt.202300398
Chemistry Europe
European Chemical Societies Publishing

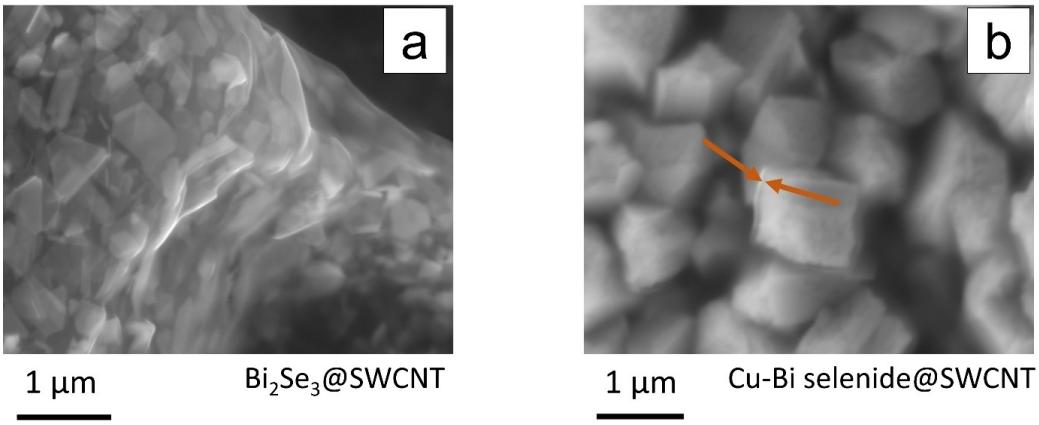

Figure 3. SEM images for the of a) Bi_2Se_3@SWCNT and b) Cu–Bi selenide@SWCNT electrodes coated with CMC layer

charging processes, and consequently, alter the electrochemical behavior of the Cu–Bi selenide@SWCNT system. These variances in polymer-crystal interactions may be related to the distinctive crystal structures of the systems.

Cyclic voltammetry (CV) measurements were conducted at a scan rate of 0.1 mV s^{-1} to analyze the side reactions occurring on the Bi_2Se_3@SWCNT and Cu–Bi selenide@SWCNT electrodes before and after coating with polymers. These measurements aimed to shed light on the electrochemical behavior of these materials during lithium-ion cycling and the impact of polymer coatings on their performance.

During the first cycle of the Bi_2Se_3@SWCNT electrode (Figure 4a), an intense cathodic peak at 0.80 V was observed, indicating the formation of a solid electrolyte interphase (SEI) layer. The cathodic peak at 2.00 V and the anodic peak at 2.29 V corresponded to Li^+ intercalation and deintercalation processes, respectively.[18] Peaks at 1.61 V and 2.01 V signified the reversible conversion of Bi_2Se_3 to Li_2Se. After the fifth cycle of the Bi_2Se_3@SWCNT electrode, the CV (Figure 4b) revealed changes in the electrochemical behavior. Instead of a peak at 0.80 V, two new peaks appeared at 0.78 V and 0.73 V, indicating the formation of LiBi and Li3Bi alloys.[45] Upon coating with polymers, the CV profiles showed less pronounced peaks, especially for alloying and dealloying reactions, suggesting that the polymer coating may reduce the rate of mass transfer in these processes. This could be attributed to a decreased availability of Li^+ ions to the active sites of the material. This change in electrochemical behavior suggests that the polymer coating enhances the stability and prolongs the charge/discharge cycle of the electrode.

In contrast to the Bi_2Se_3@SWCNT electrodes, the CV profiles for the Cu–Bi@SWCNT selenide electrode looked different (Figure 4). The cathodic peak at 2.0 V represented the intercalation of Li^+ into the copper selenide structure, forming Li_xCuSe.[41] Anodic peaks at 1.47 V corresponded to the transformation of Cu_2Se into Cu and Li_2Se,[43] while anodic peaks at 1.86 and 2.23 V indicated a multi-step formation of Cu_2Se from Cu.[43,44] The presence of bismuth in the electrode also contributed to the electrochemical processes, as evidenced by an anodic peak at 0.80 V and a cathodic peak at 0.90 V in the first cycle (Figure 4c). After the fifth cycle, a similar change in the CV profile to that observed in the Bi_2Se_3@SWCNT electrode was noticed, with two cathodic peaks appearing at 0.73 V and 0.66 V (Figure 4d). The initial CV profile for Cu–Bi selenide@SWCNT electrodes coated with polymers showed the absence of peaks at 1.88 V, indicating a change in the structure of the SEI layer (Figure 4c). However, after the fifth cycle (Figure 4d), the CV profiles for the coated and uncoated electrodes became similar, suggesting similarity in the electrochemical processes.

The capacity of the CMC-coated Bi_2Se_3@SWCNT electrode decreases already in the second cycle (Figure 5a). During second cycle the CMC-coated electrode exhibits a charging capacity of 258 mAh g^{-}1 and a discharging capacity of 196 mAh g^{-1}. Under the same conditions, the uncoated electrode demonstrates significantly higher capacities: 396 mAh g^{-1} and 320 mAh g^{-1} during charging and discharging, respectively (Figure 2e). From the second cycle the charge-discharge profiles lack clearly defined plateaus. This could suggest a potential decline in the conductivity of ions and electrons, likely due to alterations in the electrode structure. Presumably, such changes contribute to an increase in the diffusion distance for ions and electrons, resulting in a diminished capacity. In light of these findings, the decision has been made not to continue further investigations on the CMC-coated Bi_2Se_3@SWCNT. However, these results underscore the necessity for additional optimization of both the coating and structure of the electrodes to enhance their capacity and overall performance.

The Cu–Bi selenide@SWCNT electrode coated with CMC-layer (Figure 5b) shows similarity to the bare electrode profile (Figure 2f). This similarity may indicate certain properties of the electrode coating material that may be important for its operation. During the first charge-discharge cycle an additional plateau at 0.84 V is observed. This interesting phenomenon seems to be related to changes in the SEI layer caused by changes in the electrolyte. During Cu–Bi selenide@SWCNT cycling, a decrease in its capacity from the initial 798 to 449 mAh g^{-1} is noticeable (Figure 5c). However, after that, there is an increase in capacity to 730 mAh g^{-1}, which remains

Research Article
doi.org/10.1002/batt.202300398
Chemistry Europe
European Chemical Societies Publishing

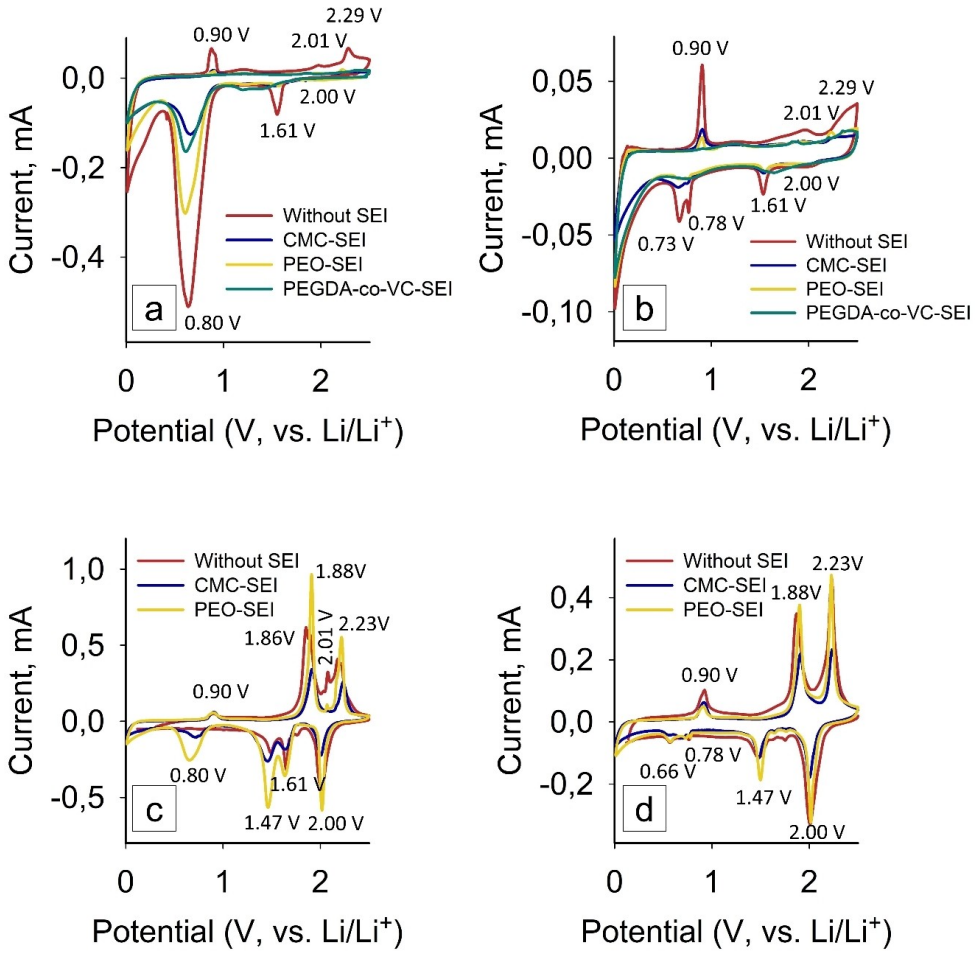

Figure 4. Cyclic voltammetry at scan rate 0.1 mV s^{-1} for a, c) the first and b, d) fifth cycles of the a, b) Bi_2Se_3@SWCNT and c, d) Cu-Bi selenide @SWCNT electrodes coated with polymer layers.

stable during the long charge / discharge cycle, carried out from the 75th to the 250th cycle.

The analysis carried out after the end of the experiment showed that the film formed after cycling has an amorphous structure and does not completely cover the electrode; on the SEM image, copper selenide crystals can be observed, which are under the polymer layer (Figure 5d). EDX data shows the presence of the elements C and O (Figure 5e), the predominance of which (Table 1) in the sample is associated with the structure of the organic CMC film. The elements Cu (copper), Bi (bismuth) and Se (selenium) refer to the electrode components. The point distribution of bismuth on EDX mapping indicates that bismuth oxide is integrated into the film structure (Figure 5f). The elements F (fluorine) and P (phosphorus) are present in electrolyte salts and, most likely, are partially incorporated into the organic layer of the film formed on the electrode during the experiment.

The charge and discharge profiles of Bi_2Se_3@SWCNT and Cu–Bi selenide@SWCNT electrodes with PEO coating (Figure 6a, b) closely resemble those of the corresponding uncoated anodes (Figure 2e, f). This indicates similar energy accumulation and release processes in both types of electrodes, which is further confirmed by the similarity in the voltammograms of coated and uncoated PEO electrodes (Figure 4). However, it is worth noting that the electrochemical properties of electrodes with PEO-SEI coating differ from those with a CMC coating. This difference is primarily evident in that the discharge capacity of both types of electrodes is significantly lower than their charge capacity, and the coulombic efficiency is around 50 % (Figures 6c, d).

This behavior may be attributed to some degree of non-uniformity in the PEO coating, which can lead to uneven lithium distribution within the electrode. This, in turn, limits the accessibility of certain areas for discharge, resulting in a reduced discharge capacity. When comparing electrodes coated with PEO and CMC, it becomes apparent that different types of coatings influence the processes of intercalation/deintercalation and the formation of the SEI layer on the surface of the electrodes, leading to differences in discharge capacity.

An important aspect of the study is the analysis of changes in the state of the polymer layer after the cycling process. The changes observed after cycling (Figures 6e–j) appear to be associated with the integration of inorganic components into the structure of the PEO-SEI layer. These changes can have a

Research Article
doi.org/10.1002/batt.202300398
Chemistry Europe
European Chemical Societies Publishing

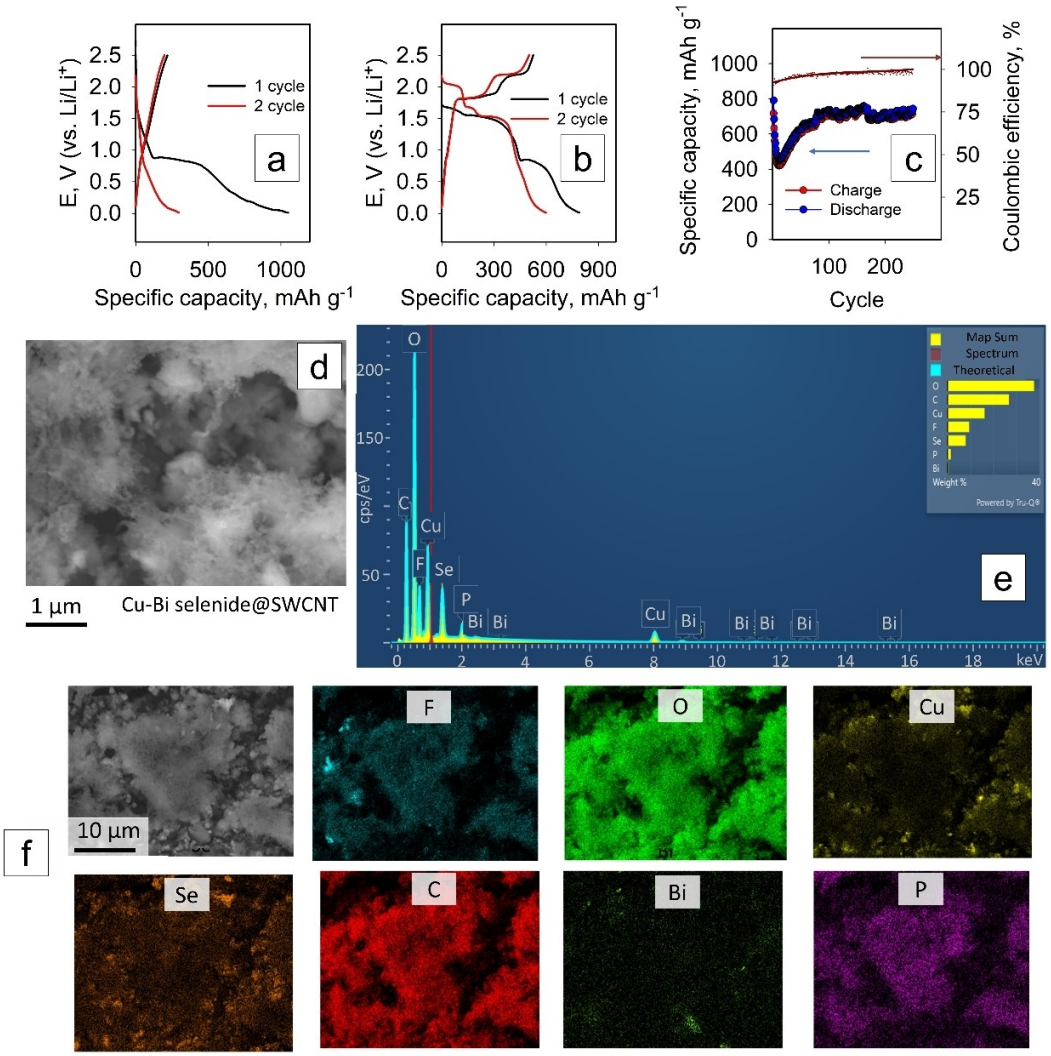

Figure 5. Charge discharge profiles of first 2 cycles of a) Bi_2Se_3@SWCNT and b) Cu–Bi selenide@SWCNT electrodes coated with CMC layer. c) Cycling performance, d) postmortem SEM images, e) postmortem EDX spectrum and f) mapping of Cu–Bi selenide@SWCNT coated with CMC layer.

significant impact on the overall performance and efficiency of the electrode.

The Bi_2Se_3@SWCNT electrode coated with a PEGDA-co-VC layer demonstrated the most stable operation in our experiments (Figure 7). At the initial cycling a slight decrease in capacity was noted. It decreased from the initial level of 460 mAh g^{-1} to 398 mAh g^{-1}. Despite this, the capacity remained stable at this level for more than 150 operating cycles. A slight increase in capacity during cycling is associated with the introduction of additional CuF_2 into the film composition. This behavior indicates the high stability of this electrode and its ability to maintain a certain level of energy over a long time period. As for the Cu–Bi selenide@SWCNT electrode, this behavior indicates that the coating of the CMC layer has similar properties to PEGDA-co-VC in terms of effect on capacitance.

Analysis of the SEM images confirms that the film covers the surface of both electrodes completely. This suggests that the film plays an important role in ensuring the stability of the electrodes.

EDX date for PEO-coated (Figures 6g–j) PEGDA-co-VC-coated electrodes (Figures 7g and h) showed C, O, Cu, Bi, Se, F and P elements as well as for CMC-layer (Figure 5e, f). Analysis of the percentage composition (Table 2) reveals the following features. Cu–Bi selenide@SWCNT electrodes coated with PEO have a high concentration of Cu (34.55) and Se (17.43) compared to other types of coatings. When coated with PEGDA-co-VC, these values decrease to 15.20 for Cu and 8.60 for Se. In Bi_2Se_3@SWCNT electrodes coated with PEGDA-co-VC, one can notice an increased concentration of O (54.81), while in the case of other coatings, the values of this element are somewhat lower. The Bi content is noticeably higher in Bi_2Se_3@SWCNT electrodes compared to Cu–Bi selenide@SWCNT for all types of coatings. For both types of electrodes, the PEGDA-co-VC coating leads to an increase in the content of C and a decrease in the content of F and P compared to other types of coatings.

Research Article
doi.org/10.1002/batt.202300398

Chemistry Europe
European Chemical Societies Publishing

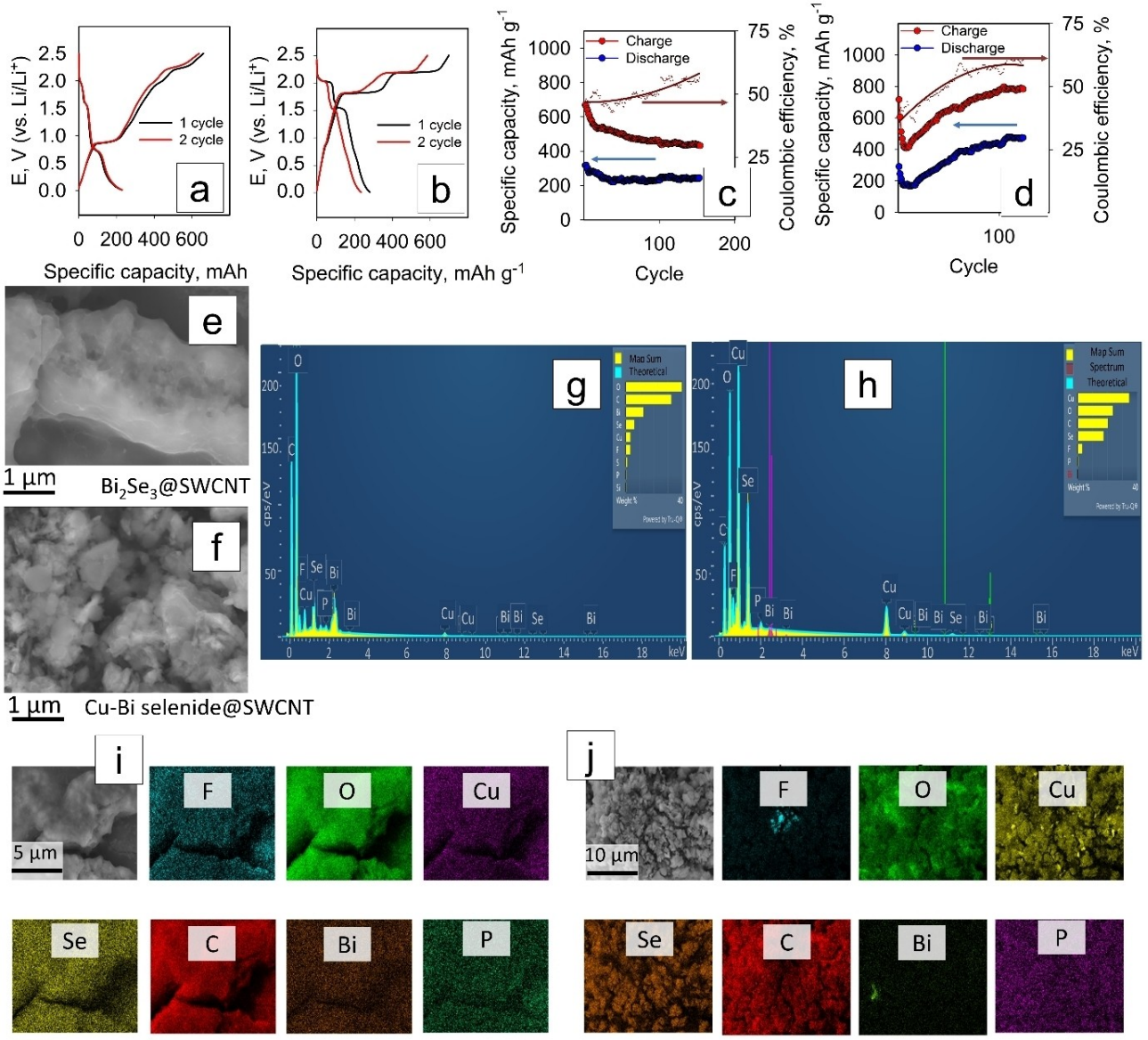

Figure 6. Charge discharge profiles of first 2 cycles of a) Bi_2Se_3@SWCNT and b) Cu–Bi selenide@SWCNT electrodes coated with PEO layer. c, d) Cycling performance, e, f) postmortem SEM images, g, h) postmortem EDX spectrum, and i, j) mapping for c, e, g, i) Bi_2Se_3@SWCNT and d, f, h, j) Cu–Bi selenide@SWCNT electrodes coated with PEO layer.

Table 2. The relative content of elements (wt%) in electrodes after cycling.

Element	Cu–Bi selenide@SWCNT			Bi_2Se_3@SWCNT	
	CMC	PEO	PEGDA-co-VC	PEO	PEGDA-co-VC
C	26.80	20.37	28.89	32.75	28.48
O	37.73	23.56	38.14	39.77	54.81
F	9.46	3.23	7.39	3.41	3.79
P	1.46	0.56	1.52	0.50	0.65
Cu	16.20	34.55	15.20	3.49	1.49
Se	7.91	17.43	8.60	7.49	4.03
Bi	0.45	0.30	0.25	12.59	6.75

Research Article
doi.org/10.1002/batt.202300398
Chemistry Europe
European Chemical Societies Publishing

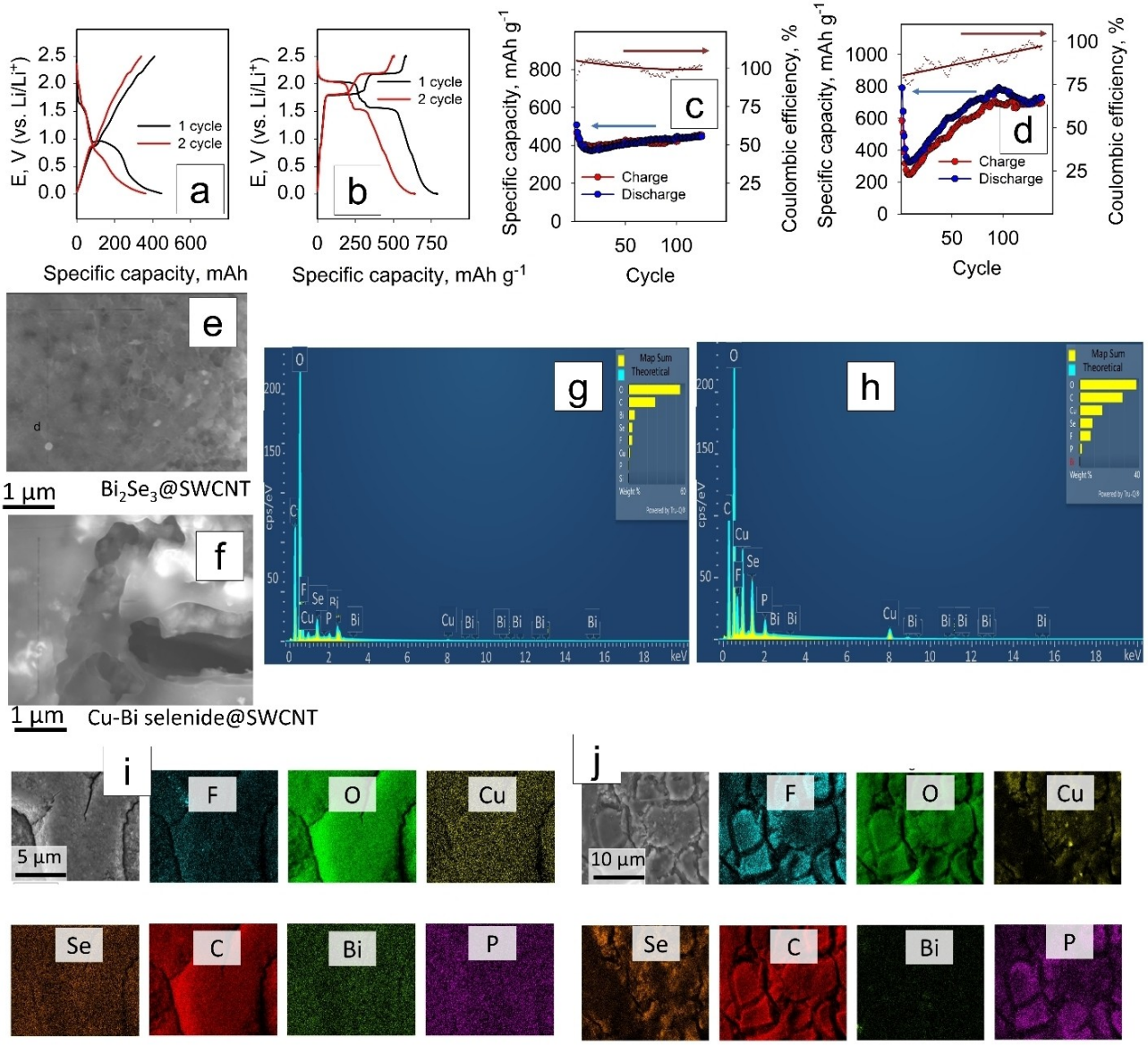

Figure 7. Charge discharge profiles of first 2 cycles of a) Bi_2Se_3@SWCNT and b) Cu–Bi selenide@SWCNT electrodes coated with PEGDA-coVC layer. c, d) Cycling performance, e, f)postmortem SEM images, g, h) postmortem EDX spectrum and i, j) mapping for c, e, g, i) Bi_2Se_3@SWCNT and d, f, h, j) Cu–Bi selenide@SWCNT electrodes coated with PEGDA-coVC layer.

Coating the electrodes with polymers and cycling performance caused a significant change in the Raman spectra, which is shown in Figures 8(a, b). According to the results of our studies, it can be seen that the Raman spectrum of the Cu–Bi selenide@SWCNT electrode after polymer coating reveals a noticeable increase in the peak at 507 cm^{-1}. This particular phenomenon indicates the presence of a strong interaction between the copper and carbon atoms, which is probably due to the modification of the chemical structure of the electrode material after coating. It can be assumed that this interaction plays an important role in the electrochemical properties of the electrode and its performance. A similar picture is also observed for the Bi_2Se_3@SWCNT electrode coated with PEGDA-co-VC. This is explained by the fact that copper fluoride was additionally introduced into the SEI structure.

The FTIR spectra (Figures 8c–e) for both Cu–Bi selenide@SWCNT and Bi_2Se_3@SWCNT electrodes with different polymer coatings showed that in all cases, after cycling, the appearance of lines at 1400 and 1436 cm^{-1}, characteristic of the -CH_2-CO- group, is observed. This indicates changes in the chemical structure of the electrode material. In addition, there is a line at 870 cm^{-1}, indicating the presence of SeO_4^{2-} in the film structure.

The fact that the spectra are similar to each other indicates that the processes occurring in the electrode material during cycling are of a common nature. Apparently, regardless of the specific type of electrode and the selected polymer coating, certain chemical reactions occur leading to the formation of these specific chemical groups.

Research Article
doi.org/10.1002/batt.202300398
Chemistry Europe
European Chemical Societies Publishing

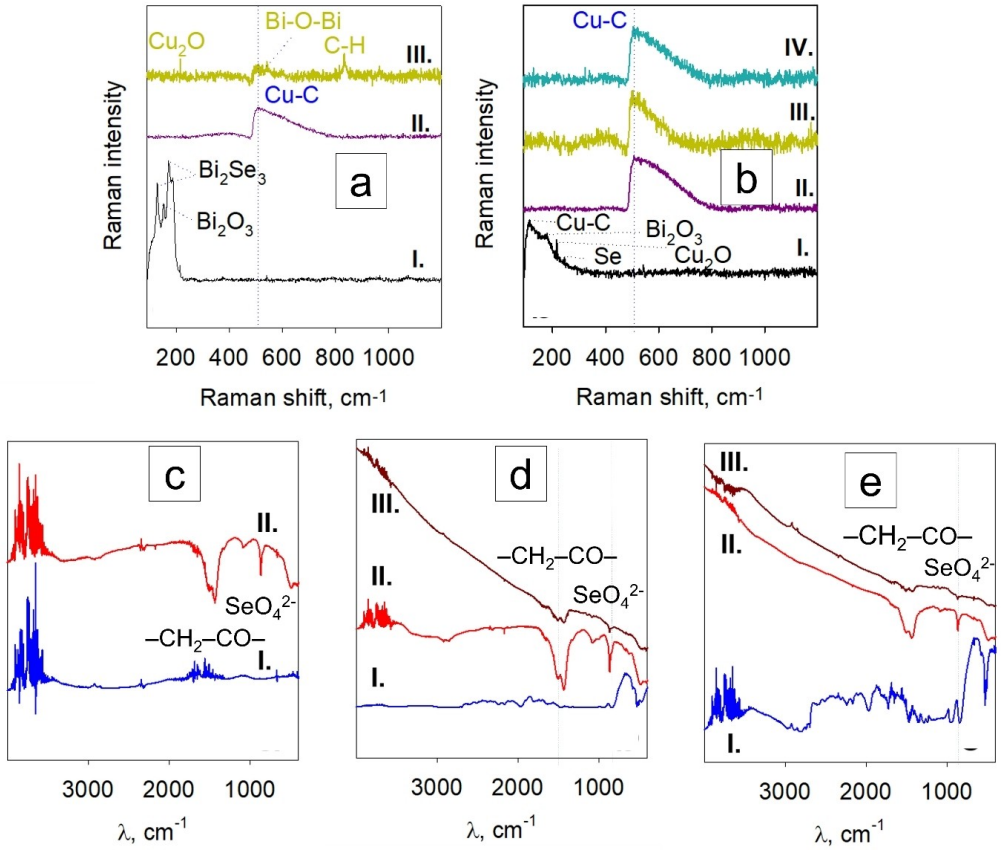

Figure 8. Raman spectra for as-prepared electrodes (I) of a) Bi_2Se_3@SWCNT and b) Cu–Bi selenide@SWCNT, and for covered electrode with PEGDA-co-VC (II), PEO (III) CMC (IV); FTIR spectra of polymers (I): c) CMC, d) PEO, e) PEGDA) and corresponding SEI layers formed on Cu–Bi selenide@SWCNT electrode (II) and Bi_2Se_3@SWCNT (III).

Conclusions

The synthesized copper selenide anode demonstrated an initial charging capacity of 478 mAh g^{-1}, but a notable decrease in capacity over the first 7 cycles was observed due to mechanical wear and the formation of decomposition products. The Bi_2Se_3@SWCNT hybrid anode exhibited a higher initial charge capacity of 853 mAh g^{-1}. After an initial decrease over the first 15 cycles, its capacity stabilized at 120 mAh g^{-1} for over 500 cycles. The bimetallic Cu–Bi selenide@SWCNT anode presented an initial charge and discharge capacity of 520 mAh g^{-1}. After a decrease in the first five cycles, the capacity showed a linear increase and remained stable.

The study also focused on the application of different conductive polymers as artificial SEI layers, namely PEO, CMC, and PEGDA-co-VC. Electrode coating with these polymers influenced the stability and efficiency of the electrodes. CMC-coated electrodes showed decreased capacities, possibly due to alterations in electrode structure. PEO-coated electrodes also presented lower discharge capacities, indicating side reactions involving the polymer. In contrast, PEGDA-co-VC-coated electrodes effectively improve Lithium-ion batteries and show notable stability and consistent capacity over numerous cycles.

Experimental Section

Synthesis of copper selenide anode. Copper selenide was synthesized by heating a mixture of 25-micron-thick copper foil (Good-Fellow Cambridge Limited) and 0.15 g of selenium (Sigma Aldrich) in a quartz tube under nitrogen. During the synthesis the temperature was raised from 20 to 585 °C over 60 minutes, followed by cooling to 475 °C, and then to room temperature.

Synthesis of Bi_2Se_3@SWCNT hybrid anode. In the first stage, a mixture of SWCNT (Ltd. Nano RAY-T) and isopropanol (Sigma-Aldrich) was sonicated, sprayed onto a glass substrate, and heated to evaporate isopropanol. In the second stage, nanostructured Bi_2Se_3 films were deposited using physical vapor deposition[46] at 585 °C under low pressure before cooling to 470 °C. Then samples with mass ratio of Bi_2Se_3 to SWCNT = 2:1 were cooled to room temperature and attached to copper substrates.

Synthesis of bimetallic Cu-Bi selenide@SWCNT anode. The bimetallic Cu–Bi selenide@SWCNT anode was synthesized similarly to the Bi_2Se_3@SWCNT anode but using a 25-micron copper foil substrate instead of glass. After applying a SWCNT-isopropanol suspension to the foil, a Bi_2Se_3 film was deposited at 585 °C in a GCL-1100X

furnace. A significant difference was that copper from the substrate replaces bismuth in the process, forming microcrystals of Cu_2Se, alloyed with Bi.[47]

Formation of the artificial polymer SEI-layers. Polyethylene oxide (PEO, molecular weight 100,000, Sigma Aldrich), carboxymethyl cellulose (CMC, Carboxymethylcellulose sodium salt, medium viscosity, Sigma Aldrich), and a copolymer of poly(ethylene glycol) diacrylate and vinylene carbonate (PEGDA-co-VC) were used to create the artificial SEI layers. For PEO-SEI and CMC-SEI layers, PEO and CMC were dissolved in water, then spin-coated onto electrodes at 3000 rpm for 15 minutes and dried at 60 °C. For the PEGDA-co-VC layer, PEGDA (PEGDA, Mr 20000) and vinylene carbonate (VC, Vinylene carbonate solution 1.0 M in ethyl acetate, Sigma Aldrich) were mixed with CuF_2 and $LiNO_3$ in dimethyl carbonate.[48] This mixture was applied to the electrode and cured under UV light (365 nm) for 15 minutes.

Testing and analysis. Electrochemical properties were studied using CR2032-type half-cells with lithium foil electrodes and a 1 M $LiPF_6$ electrolyte. The separator was Celgard 2320. Assembly occurred in an argon-filled glove box with O_2 and H_2O under 0.5 ppm. Electrochemical measurements were made using the Bilologic battery testing system (BCS-800).

The electrode's characteristics were assessed via X-ray diffractometry (XRD, X'PERT PRO MPD Alpha1), scanning electron microscopy (SEM), and energy-dispersive X-ray (EDX) techniques (JEOL JIB-4700F). Changes in the electrodes were investigated post-disassembly of the coin cells in an Ar-filled glovebox.

SEI layers were evaluated using Raman spectroscopy (Renishaw in Via Qontor) and FTIR (PerkinElmer FT-IR/FIR Spectrometer). For FTIR, samples were prepared using KBr pellets.

Acknowledgements

This research was funded by the European Regional Development Fund Project No. 1.1.1.2/VIAA/4/20/694; V.L. also acknowledges "Strengthening of the capacity of doctoral studies at the University of Latvia within the framework of the new doctoral model", identification No. 8.2.2.0/20/I/006.

Conflict of Interests

The authors declare no conflict of interest.

Data Availability Statement

The data that support the findings of this study are available from the corresponding author upon reasonable request.

Keywords: copper selenide · carbon nanotubes · bimetallic Cu–Bi selenide · conductive polymers · artificial solid electrolyte interface

[1] J. F. Peters, M. Baumann, B. Zimmermann, J. Braun, M. Weil, *Renewable Sustainable Energy Rev.* **2017**, *67*, 491–506.
[2] D. Deng, *Energy Sci. Eng.* **2015**, *3*, 385–418.
[3] V. Etacheri, R. Marom, R. Elazari, G. Salitra, D. Aurbach, *Energy Environ. Sci.* **2011**, *4*, 3243.
[4] C. M. Hayner, X. Zhao, H. H. Kung, *Annu. Rev. Chem. Biomol. Eng.* **2012**, *3*, 445–471.
[5] N. Nitta, F. Wu, J. T. Lee, G. Yushin, *Mater. Today* **2015**, *18*, 252–264.
[6] H. Li, Z. Wang, L. Chen, X. Huang, *Adv. Mater.* **2009**, *21*, 4593–4607.
[7] Y. Mekonnen, A. Sundararajan, A. I. Sarwat, in *SoutheastCon 2016*, IEEE, **2016**, pp. 1–6.
[8] L. Huang, S. Shen, Y. Zhong, Y. Zhang, L. Zhang, X. Wang, X. Xia, X. Tong, J. Zhou, J. Tu, *Adv. Mater.* **2022**, *34*, DOI 10.1002/adma.202107415.
[9] C. de las Casas, W. Li, *J. Power Sources* **2012**, *208*, 74–85.
[10] P. E. Lokhande, A. Pakdel, H. M. Pathan, D. Kumar, D.-V. N. Vo, A. Al-Gheethi, A. Sharma, S. Goel, P. P. Singh, B.-K. Lee, *Chemosphere* **2022**, *297*, 134225.
[11] J. Tao, Z. Yan, J. Yang, J. Li, Y. Lin, Z. Huang, *Carbon Energy* **2022**, *4*, 129–141.
[12] C. Jiang, E. Hosono, H. Zhou, *Nano Today* **2006**, *1*, 28–33.
[13] E. Pomerantseva, F. Bonaccorso, X. Feng, Y. Cui, Y. Gogotsi, *Science* **2019**, *366*, 1–12.
[14] I. Hasa, J. Hassoun, S. Passerini, *Nano Res.* **2017**, *10*, 3942–3969.
[15] H. Yuan, L. Kong, T. Li, Q. Zhang, *Chin. Chem. Lett.* **2017**, *28*, 2180–2194.
[16] I. Hussain, S. Sahoo, C. Lamiel, T. T. Nguyen, M. Ahmed, C. Xi, S. Iqbal, A. Ali, N. Abbas, M. S. Javed, K. Zhang, *Energy Storage Mater.* **2022**, *47*, 13–43.
[17] V. Lazarenko, Y. Rublova, R. Meija, J. Andzane, V. Voikiva, A. Kons, A. Sarakovskis, A. Viksna, D. Erts, *Batteries* **2022**, *8*, 144.
[18] G. Han, Z. Chen, D. Ye, L. Yang, L. Wang, J. Drennan, J. Zou, *J. Mater. Chem. A* **2014**, *2*, 7109.
[19] R. Singh, P. Kumari, M. Kumar, T. Ichikawa, A. Jain, *Molecules* **2020**, *25*, 3733.
[20] J. Ni, X. Bi, Y. Jiang, L. Li, J. Lu, *Nano Energy* **2017**, *34*, 356–366.
[21] Y. Zhang, Q. Zhou, J. Zhu, Q. Yan, S. X. Dou, W. Sun, *Adv. Funct. Mater.* **2017**, *27*, 1–34.
[22] S. C. Singh, H. Li, C. Yao, Z. Zhan, W. Yu, Z. Yu, C. Guo, *Nano Energy* **2018**, *51*, 774–785.
[23] D. Chen, G. Chen, R. Jin, H. Xu, *CrystEngComm* **2014**, *16*, 2810.
[24] S. H. Yang, S. Park, G. D. Park, J. Lee, Y. C. Kang, *Small* **2020**, *16*, 2002345.
[25] M. Zhang, Y. Liu, Y. Zhang, X. Bai, H. Zhu, X. Li, Y. Liu, D. Cui, B. Li, X. Tao, *ChemElectroChem* **2020**, *7*, 139–147.
[26] T. Yang, M. Fang, J. Liu, D. Yang, Y. Liang, J. Zhong, Y. Yuan, Y. Zhang, X. Liu, R. Zheng, K. Davey, J. Zhang, Z. Guo, *Adv. Funct. Mater.* **2022**, *32*, 2205880.
[27] Y. Zhu, H. Tang, X. Yun, L. Xi, Z. Hu, *J. Alloys Compd.* **2021**, *866*, 158972.
[28] Y. Kang, C. Deng, Y. Chen, X. Liu, Z. Liang, T. Li, Q. Hu, Y. Zhao, *Nanoscale Res. Lett.* **2020**, *15*, 112.
[29] D.-H. Ha, M. A. Islam, R. D. Robinson, *Nano Lett.* **2012**, *12*, 5122–5130.
[30] S. H. Ng, J. Wang, Z. P. Guo, J. Chen, G. X. Wang, H. K. Liu, *Electrochim. Acta* **2005**, *51*, 23–28.
[31] X. Zhu, X. Wu, T. N. L. Doan, Y. Tian, H. Zhao, P. Chen, *J. Power Sources* **2016**, *326*, 498–504.
[32] X. Shan, Y. Zhong, L. Zhang, Y. Zhang, X. Xia, X. Wang, J. Tu, *J. Phys. Chem. C* **2021**, *125*, 19060–19080.
[33] S. Gao, F. Sun, N. Liu, H. Yang, P.-F. Cao, *Mater. Today* **2020**, *40*, 140–159.
[34] M. B. McDonald, P. T. Hammond, *ACS Appl. Mater. Interfaces* **2018**, *10*, 15681–15690.
[35] Y. Shi, L. Peng, Y. Ding, Y. Zhao, G. Yu, *Chem. Soc. Rev.* **2015**, *44*, 6684–6696.
[36] V. Lazarenko, R. Meija, Y. Rublova, A. Kons, V. Voikiva, J. Andzane, R. Lohmus, A. Sarakovskis, X. Kong, T. Kallio, A. Viksna, D. Erts, *Manuscript submitted for publication* **2023**.
[37] J.-F. Ding, R. Xu, C. Yan, B.-Q. Li, H. Yuan, J.-Q. Huang, *J. Energy Chem.* **2021**, *59*, 306–319.
[38] E. Peled, S. Menkin, *J. Electrochem. Soc.* **2017**, *164*, A1703–A1719.
[39] P. Kumari, R. Singh, K. Awasthi, T. Ichikawa, M. Kumar, A. Jain, *J. Alloys Compd.* **2020**, *838*, 155403.
[40] D. Yu, X. Wei, D. Zhao, S. Gao, G. Zhao, H. Zhang, Z. Li, M. Yu, Y. Sun, *Electrochim. Acta* **2022**, *404*, 139703.
[41] J. Xiao, H. Liu, J. Huang, Y. Lu, L. Zhang, *Appl. Surf. Sci.* **2020**, *526*, 146746.
[42] Y. Jiang, M. Xie, F. Wu, Z. Ye, Y. Zhang, Z. Wang, Y. Zhou, L. Li, R. Chen, *Small* **2021**, *17*, 2102893.
[43] K. Zhu, S. Wei, Q. Zhou, S. Chen, Y. Lin, P. Zhang, Y. Cao, C. Wang, Y. Wang, Y. Xia, D. Cao, Z. Mohamed, X. Guo, X. Yang, X. Wu, L. Song, *Nano Res.* **2023**, *16*, 2421–2427.

[44] H. Li, J. Jiang, F. Wang, J. Huang, Y. Wang, Y. Zhang, J. Zhao, *ChemSusChem* **2017**, *10*, 2235–2241.
[45] R. Jin, M. Sun, G. Li, *Ceram. Int.* **2017**, *43*, 17093–17099.
[46] J. Andzane, A. Felsharuk, A. Sarakovskis, U. Malinovskis, E. Kauranens, M. Bechelany, K. A. Niherysh, I. V. Komissarov, D. Erts, *Mater. Today Energy* **2021**, *19*, 100587.
[47] Y. Takagaki, U. Jahn, M. Ramsteiner, K.-J. Friedland, *Semicond. Sci. Technol.* **2011**, *26*, 085031.
[48] W. Lu, L. Sun, Y. Zhao, T. Wu, L. Cong, J. Liu, Y. Liu, H. Xie, *Energy Storage Mater.* **2021**, *34*, 241–249.

Manuscript received: September 12, 2023
Revised manuscript received: November 15, 2023
Accepted manuscript online: November 17, 2023
Version of record online: December 6, 2023